



# Prediction of the excited-state reaction channels in photo-induced processes of nitrofurantoin using first-principle calculations and dynamics simulations

Kunni Lin <sup>a</sup>, Deping Hu <sup>b</sup>, Jiawei Peng <sup>b</sup>, Chao Xu <sup>a</sup>, Feng Long Gu <sup>a, \*\*</sup>, Zhenggang Lan <sup>b,\*</sup>

<sup>a</sup> Key Laboratory of Theoretical Chemistry of Environment, Ministry of Education, School of Chemistry, South China Normal University, Guangzhou, 510006, PR China

<sup>b</sup> Guangdong Provincial Key Laboratory of Chemical Pollution and Environmental Safety and MOE Key Laboratory of Environmental Theoretical Chemistry, SCNU Environmental Research Institute, School of Environment, South China Normal University, Guangzhou, 510006, PR China

## ARTICLE INFO

Handling Editor: Jun Huang

**Keywords:**  
Photochemistry  
Theoretical studies  
Nitrofurantoin  
Reaction channels

## ABSTRACT

The understanding of the photochemistry of antibiotic compounds is important because it gives the direct information on the possible environmental pollution caused by them. Due to their large size, the theoretical studies of their excited-state reactions are rather challenging. In current work, we combined the on-the-fly trajectory surface-hopping dynamics, conical-intersection optimizations and excited-state pathway calculations to study the photochemistry of the *trans*-isomer of nitrofurantoin, a widely-used drug to treat the urinary tract infections. The dynamics-then-pathway approach was taken. First the trajectory surface hopping dynamics at the state-averaged complete-active-space self-consistent-field (SA-CASSCF) level with small active space and small basis sets were run. Second, the minimum-energy conical-intersection optimizations were performed. Finally the excited pathways from the Frank-Condon region to different reaction channels were built at the multi-state multi-reference second-order perturbation (MS-CASPT2) level with large active space and large basis set. Several possible channels responsible for the photo-induced reaction mechanism of the *trans*-nitrofurantoin were obtained, including the cleavage of the NO bond of the NO<sub>2</sub> moiety, the photoisomerization at the central CN bond, and other internal conversion channels. Our findings give some preliminary explanations on available experimental observations. It is also demonstrates that the current theoretical approach is a powerful tool to explore the excited-state reactions in the photochemistry of media-sized or large-sized drug compounds.

## 1. Introduction

The photochemistry of pollutant molecules is one of the essential topics in environmental sciences (Wayne, 2005; Boule, 2013; Bahne-mann and Robertson, 2015). The antibiotic drug compounds emerge as a new group of pollutant molecules (Albini and Fasani, 2007; Liu et al., 2009; Ge et al., 2010b, 2019; Homem and Santos, 2011; Chen et al., 2014; Hoseini et al., 2014; Tripathi and Tripathi, 2017; Lastre-Acosta et al., 2020) and the understanding of their potential-environmental toxicity becomes important. The photochemistry of these molecules received considerable research interests (Albini and Fasani, 2007; Ge et al., 2010b, 2019; García-Galán et al., 2012; Challis et al., 2013; Chen et al., 2014; Hong et al., 2016; Lastre-Acosta et al., 2020). For instance, several works tried to explore the chemical reactions between these

compounds and photo-generated radicals and their possible reactions on triplet states (Lorenzo et al., 2008, 2009, 2009; Ge et al., 2010a; Chen et al., 2014; Li et al., 2014; Xu et al., 2014; Parra et al., 2017; Lastre-Acosta et al., 2020). The direct photo-induced reactions also take place in many antibiotic drug compound families (Edhlund et al., 2006; Werner et al., 2006, 2007; Chen et al., 2008), such as macrolides antibiotics, nitrofuran antibiotics and tetracyclines. For instance, nitrofurans (such as furazolidone) and macrolides (such as tylosin) first experience the rapid photoisomerization under sunlight and then undergo the photodegradation (Edhlund et al., 2006; Werner et al., 2007). The photolysis reaction of tetracycline antibiotics was also confirmed in references (Werner et al., 2006; Chen et al., 2008).

Compared to the many experimental researches on the photochemical reaction of antibiotics (Edhlund et al., 2006; Werner et al., 2006,

\* Corresponding author.

\*\* Corresponding author.

E-mail addresses: [gu@scnu.edu.cn](mailto:gu@scnu.edu.cn) (F.L. Gu), [zhenggang.lan@m.scnu.edu.cn](mailto:zhenggang.lan@m.scnu.edu.cn), [zhenggang.lan@gmail.com](mailto:zhenggang.lan@gmail.com) (Z. Lan).

2007; Chen et al., 2008, 2014; Lorenzo et al., 2008, 2009, 2009; Ge et al., 2010a; Li et al., 2014; Xu et al., 2014; Parra et al., 2017; Lasstre-Acosta et al., 2020; Szabó-Bárdos et al., 2020), the theoretical studies on this topic are still quite limited. A few of theoretical works(Wei et al., 2013; Li et al., 2015, 2016a, 2016b) mainly focus on either the triplet-state reactions or the reactions between the ground-state antibiotics molecules and the radicals generated by the light. As the contrast, much less efforts were made in the understanding of the photo-induced reactions that directly involves the excited states of the antibiotics compounds. However, the theoretical investigations on the excited-state potential energy surfaces (PESs) and the simulations of excited-state dynamics of antibiotic compounds are certainly very helpful. These simulations not only give the direct understanding of their photochemistry at atomic level, but also provide the useful information to clarify their potentially environmental influences. For instance, very recently Granucci and co-workers employed the trajectory surface hopping (TSH) dynamics at the semiempirical AM1/CIS level to study the excited-state dynamics of nonsteroidal anti-inflammatory drugs (Aguilera-Porta et al., 2019). This work predicted the excited state lifetime of five medical substances including aspirin, ibuprofen, carprofen, suprofen and indomethacin. Some key molecular motions responsible for the nonadiabatic decay, such as ring puckering, were identified. Overall, the theoretical simulations on the excited-state pathways and dynamics are powerful tools to study photo-induced reactions of medicine compounds, which should be useful to help environmental scientists to understand the potential environmental effects of the antibiotic drug compounds.

Nitrofurantoin is a widely-used drug in the medical treatment of urinary tract infections(Bailey et al., 1971; Gleckman et al., 1979; Guay, 2001; Gupta et al., 2007; Singh et al., 2015). This compound experiences complicated photo-induced processes, and the detailed mechanisms of the excited-state reactions are still not fully clear. A few works proposed various photo-induced reaction channels(Edhlund et al., 2006; Parra et al., 2017; Szabó-Bárdos et al., 2020), including the photo-induced isomerization, the fragmentation into nitrofuraldehyde and amino-hydantoin, the re-arrangement of the NO<sub>2</sub> group, etc. For instance, Edhlund et al. proposed that the isomerization at the central CN bond takes place for nitrofurantoin in aquatic solution after photoabsorption (Edhlund et al., 2006). At the same time, other furan derivatives, such as furaltadone and furazolidone, also display the similar photo-induced isomerization reactions(Edhlund et al., 2006). However, quite limited knowledge was accumulated for their photochemical reactions at the atomic level. To get a microscopic understanding on the potential environment risk of nitrofuran family, the theoretical investigation on their photo-induced reactions mechanism should be helpful.

The theoretical study on the photochemistry of nitrofuran family represents a typical challenging in this field. These compounds have many nuclear degrees of freedom and their photochemistry involves several coupled electronic states, thus the employment of the high-level ab initio methods for the accurate treatment of these compounds is quite challenging. In addition, the pre-known knowledge on the reaction mechanism of their photochemistry is highly missing. It is well known that conical intersection (CI) is the “funnel” of the photochemistry of polyatomic systems(Domcke et al., 2004, 2011), while we do not have any information to identify the relevant CIs in the photochemistry of the nitrofuran family compounds.

In this work, we tried to investigate the photo-induced excited-state reaction processes of nitrofurantoin, which is a prototype compound in nitrofuran family, from the theoretical point of view. Here the dynamics-then-pathway approach was taken. The main purpose of the current work is to build the reaction pathways on the molecular excited states. To obtain the basic ideas on the active coordinates, we first employed the on-the-fly TSH simulation(Cattaneo and Persico, 2001; Barbatti et al., 2007; Fabiano et al., 2008; Lan et al., 2009; Barbatti, 2011; Richter et al., 2011; Wohlgemuth et al., 2011; Du and Lan, 2015a, 2015b; Kranz and Elstner, 2016; Mai et al., 2018; Persico and Granucci, 2018) starting from the low-lying excited states was computed at the SA-CASSCF level with the smaller active space and basis set. Here various initial conditions with different initial energy were considered to obtain possible internal conversions and

Tully’s fewest-switches algrothim(Tully, 1990) to clarify the relevant decay channels. In the TSH simulation, we chose the state-averaged complete-active-space self-consistent-field (SA-CASSCF) approach (Roos and Lawley, 1987) with smaller active space, smaller basis set and the limited number of averaged states. After the TSH calculations, we analyzed the photolysis channels and the internal conversion channels with the unsupervised machine learning approaches, the classical multi-dimensional scaling (MDS) dimensionality reduction method(De Silva and Tenenbaum, 2004; Borg and Groenen, 2005; Härdle, 2015) and the K-means clustering analysis(Hartigan and Wong, 1979; Jain, 2010). The CIs responsible for the internal conversion dynamics to the ground state were optimized from the representative hopping geometries. The reaction pathways of the internal conversion channels to the ground state and the photolysis channels towards the photo-dissociation products were built at the multi-state multi-reference second-order perturbation (MS-CASPT2) level(Andersson et al., 1990, 1992), which were calculated with the large active space, the reasonable basis set and the large number of electronic states in the state-averaged calculations. After the construction of the excited-state pathways, the photo-induced mechanism was addressed. This work not only provided a detailed understanding of the photochemistry of nitrofurantoin, but also demonstrated that the dynamics-then-pathway approach might be an efficient tool to study the photochemistry of drug compounds in the future. This paper is organized as follows. Section II discusses all theoretical and computational details; Section III discusses all results and Section IV gives the summary of this work.

## 2. Theoretical methods and computational details

The study of the photo-induced excited-state processes of nitrofurantoin is not a trivial task. As discussed in the above and below sections, the photochemistry of nitrofurantoin is very rich. The bright state responsible for the photo-absorption is not the first or second electronic state, and thus many electronic states are involved in the photochemistry. To deal with such processes, we face two problems.

When the high-level quantum chemistry approaches (such as SA-CASSCF and MS-CASPT2 approaches) were employed in the current study, the suitable basis sets, the reasonable active space and the proper state-averaged calculations should be chosen. In the current studies, several electronic states that play the essential roles in the photochemistry of nitrofurantoin should be taken into account in the calculations. For convergence, we even need to include more electronic states in the state-averaged calculations to get the smooth PESs in the construction of the excited-state pathways. Also due to the large system size and complicated electronic transitions, we expect the selection of the active space becomes not trivial. At the same time, we do not have the enough knowledge of reactive coordinates, relevant CIs and possible channels. However, the lack of the reactive coordinate prevents us to build the excited-state reaction pathways.

The above two problems bring challenges in the theoretical study of the excited-state reaction channels of the current system. Although the employment of the direct nonadiabatic dynamics simulation with many electronic states and rather large active spaces may automatically solve them, the computational cost is very high for nitrofurantoin.

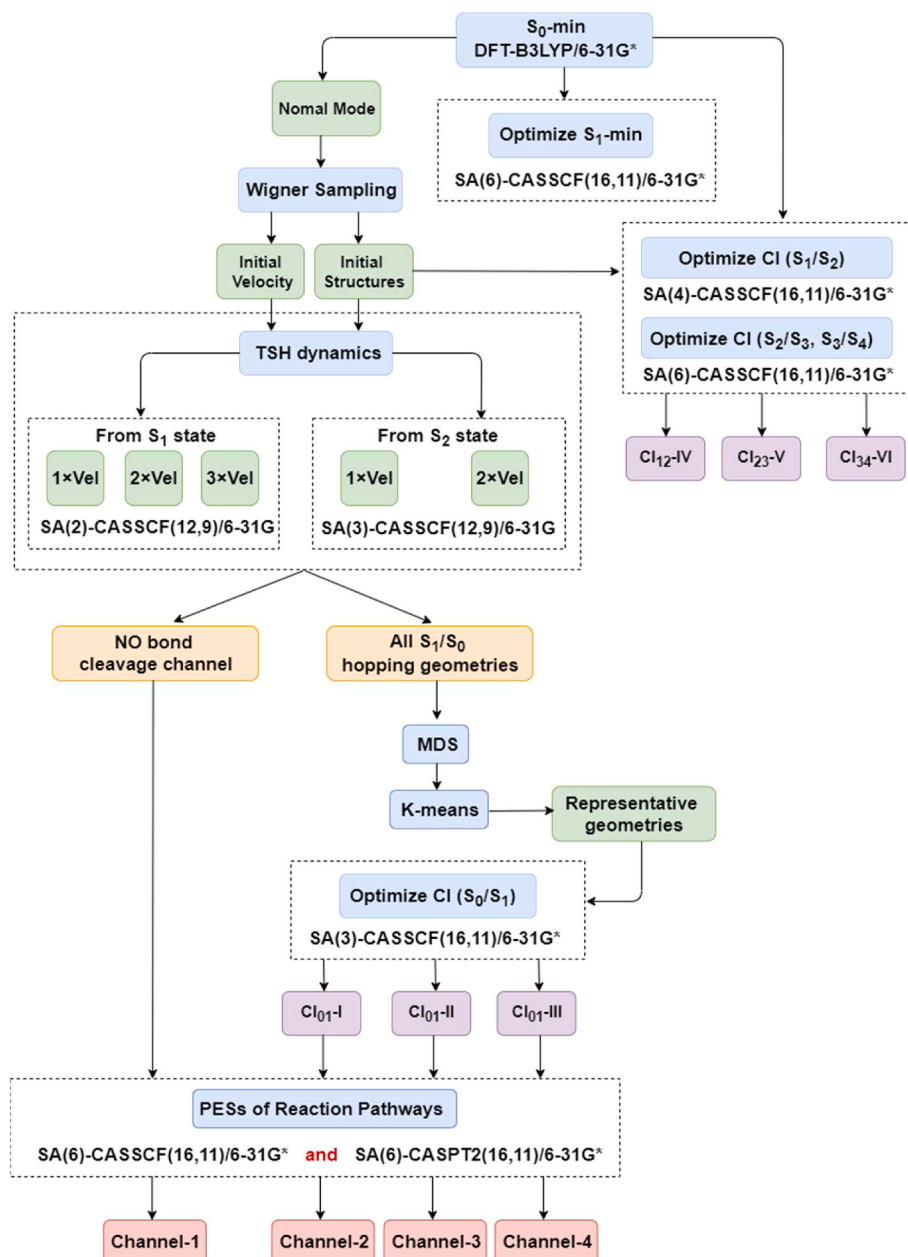
To get a reasonable description of the photochemistry of nitrofurantoin, we took the dynamics-then-pathway approach here. We first ran the preliminary nonadiabatic dynamics to obtain the rough ideas on the reaction channels with a reasonable computational cost. In this step, the on-the-fly Tully’s fewest-switches TSH dynamics(Tully, 1990; Cattaneo and Persico, 2001; Barbatti et al., 2007; Fabiano et al., 2008; Lan et al., 2009; Barbatti, 2011; Richter et al., 2011; Wohlgemuth et al., 2011; Du and Lan, 2015a, 2015b; Kranz and Elstner, 2016; Mai et al., 2018; Persico and Granucci, 2018) starting from the low-lying excited states was computed at the SA-CASSCF level with the smaller active space and basis set. Here various initial conditions with different initial energy were considered to obtain possible internal conversions and

photolysis pathways. The geometrical features of all S<sub>1</sub>-S<sub>0</sub> hops were analyzed using the unsupervised machine learning approaches, the classical MDS dimensionality reduction method (Borg and Groenen, 2005; Härdle, 2015) and K-means clustering analysis (Hartigan and Wong, 1979; Jain, 2010). Starting from the hopping geometries, the S<sub>0</sub>/S<sub>1</sub> CIs were optimized. Next, we assumed that the internal conversion dynamics of nitrofuranoin is mainly via these S<sub>0</sub>/S<sub>1</sub> surface crossings. In principle, this assumption should be reasonable. Because of the presence of excited-state CIs (see below discussions), the system quickly decays to the lower electronic states and such relaxation dynamics in principle should be rather fast due to the large number of vibrational degrees of freedom. After the knowledge of the internal conversion dynamics towards the ground state and the photolysis channels were known, the reaction pathways from the FC region to the relevant CIs or photolysis products were built at the SA-CASSCF and MS-CASPT2 levels with the large active space, more electronic states and reasonable basis set. The current simulation protocol provided a good balance between

computational efficiency and accuracy.

Below we explain the computational procedures step by step. At the same time, we provided a brief flow chart of all steps in **Scheme 1**.

- (a) The ground-state minimum-energy geometries (S<sub>0</sub>-min) were optimized at the DFT-B3LYP/6-31G\* level. The vertical excitation at the ground state minimum is calculated at the SA(6)-CASSCF(16,11)/6-31G\* and SA(6)-MS-CASPT2(16,11)/6-31G\* levels including six  $\pi$  orbitals, three  $\pi^*$  orbitals and two n orbitals. The active space was given in Fig. S1 in Supporting Information (SI). Here, six electronic states were taken into account in the SA(6)-CASSCF and MS(6)-CASPT2 calculations.
- (b) The trial nonadiabatic dynamics simulations were performed using the on-the-fly Tully's fewest-switches TSH method. The main purpose of this step was to find possible reaction channels with low computational cost. Here, the SA-CASSCF(12,9)/6-31G level was chosen. In principle, the photochemistry of



**Scheme 1.** The flow chart of all steps in our work.

nitrofuranoin starts from the higher electronic states. If all relevant electronic states were taken into account in the current TSH step, the computational cost becomes extremely high and the convergence is also a serious problem. As a compromise solution, the current TSH calculations started only from the low-lying electronic states, while we need to find all possible channels including those responsible for the high initial-energy cases. To deal with this problem, we tried to use various initial conditions in the TSH calculations. The coordinates and velocities were sampled by the Wigner distribution function of the lowest vibrational level of the ground electronic state(Wigner, 1932; Barbatti et al., 2007; Tannor, 2007; Du and Lan, 2015a, 2015b). These initial conditions were put into the first excited state ( $S_1$ ) vertically and the on-the-fly TSH dynamics was calculated at the SA(2)-CASSCF(12,9)/6-31G level. Next, we kept all sampled geometries unchanged, while multiplied the velocities by the factors of 2 and 3. In test calculations, when this factor reaches to 3, all trajectories gives the O-atom detachment channel due to too much initial kinetic energy. Therefore, we only considered the constant factors not more than 3. Certainly, the high initial energy may also be achieved by the sampling with high temperature. However, if we performed the Wigner sampling with high temperature, the geometry distortion becomes more significant and some unphysical geometries may appear. As a contrast, the enlargement of the velocities within the current sampling procedure only results in the higher initial kinetic energy, while the sampled geometries remain unchanged. This indicates that the current sampling approach confirmed the correct geometry distribution in the Frank-Condon region. Based on these new initial conditions, the TSH dynamics from the  $S_1$  state was simulated again. The same procedure was performed in the TSH simulation at the SA(3)-CASSCF(12,9)/6-31G level to study the nonadiabatic dynamics starting from the second excited state ( $S_2$ ). The above approaches provided us more reaction channels with different initial energies, which may be involved in the photochemistry of nitrofuranoin. In all cases, the trajectory propagation lasts 1.5 ps, and the time steps for the propagation of nuclear and electronic motions are 0.5 fs, 0.005 fs, respectively. The decoherence correction was taken into account(Granucci and Persico, 2007). Finally, the hopping geometries for all TSH dynamics are collected. The above sets of Tully's fewest-switches TSH dynamics provided us the excited-state dynamics channels, including the photolysis and the internal conversion channels.

(c) To obtain the possible CIs responsible for the  $S_0/S_1$  internal conversion in the nonadiabatic dynamics, we examined the geometrical features at hops with unsupervised machine learning approaches, namely dimensional reduction(Rohrdanz et al., 2013) and clustering(Hartigan and Wong, 1979; Sarle et al., 1991). After the  $S_1-S_0$  hopping geometries were collected, the classical MDS (De Silva and Tenenbaum, 2004; Borg and Groenen, 2005; Härdle, 2015) method was used to analyze their geometry features. The details of MDS were found in our previous works(Li et al., 2017, 2018). Then the K-means clustering approach(Hartigan and Wong, 1979; Jain, 2010) was used to divide the relevant hopping geometries into several groups. The K-means clustering algorithm automatically determines the coordinates of the center of each clusters by iteration. In a specified cluster, the data point that shows the smallest distance to the cluster center was located in the reduced space. The corresponding geometry was assigned as the representative geometry in this cluster. These typical hopping geometries were taken as the initial guess to perform the  $S_0/S_1$  CI optimizations at the SA-CASSCF level. In addition, we randomly chose several geometries in the FC region to optimize the CIs between excited states. All CI optimizations were performed at the level of SA-CASSCF(16,11)/6-31G\* to obtain the CIs with high accuracy.

Different state-averaged calculations were taken here mainly due to the balances of computational cost, convergence issues and accuracy.

(d) The excited-state reaction pathways towards the photolysis and internal conversion channels were built at the SA(6)-CASSCF (16,11)/6-31G\* and SA(6)-MS-CASPT2(16,11)/6-31G\* levels.

The DFT calculation was performed using the Gaussian16 package(Frisch et al., 2016). The TSH calculations were performed by our home-made JADE-NAMD code(Du and Lan, 2015a, 2015b; Hu et al., 2017) that contains the interface between the TSH dynamics and the SA-CASSCF calculations of the Molpro package(Werner et al., 2012, 2020). All MS-CASPT2 calculations were performed using the Open-Molcas package(F. Galván et al., 2019; Aquilante et al., 2020).

### 3. Results and discussion

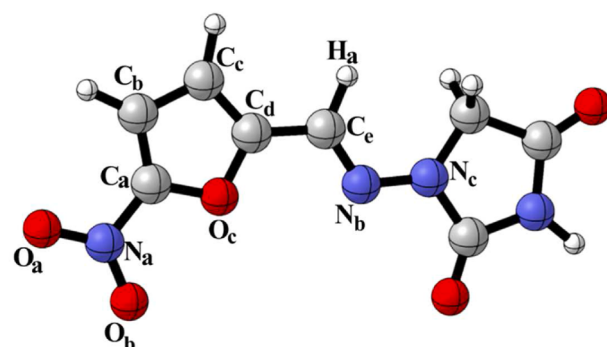
#### 3.1. Basic information of molecular structure

The molecular structure of nitrofuranoin along with the atomic labels is shown in Scheme 2. All important atoms playing important roles in the excited-state reactions are labelled by their atomic names with the alphabetic order. For instances,  $O_a$  and  $O_b$  represent two O atoms of the  $NO_2$  group. All key internal coordinates are listed in Table 1. The distances  $r_a$ ,  $r_b$ ,  $r_c$  describe the  $C_a-N_a$ ,  $N_a-O_a$ ,  $N_a-O_b$  stretching motion, respectively. The dihedral angles  $\tau_a$  and  $\tau_b$  reflect the internal rotation motion of  $NO_2$  group. The dihedral angles  $\tau_c$ ,  $\tau_d$  and  $\tau_e$ , reflect the torsional motion along with  $C_eN_b$  bond, the pyramidalization motion at the  $C_e$  atom and  $N_a$  atom, respectively. The dihedral angle  $\tau_f$  ( $C_b-O_c-C_a-N_a$ ) characterizes the out-of-plane motion at the  $NO_2$  group with respect to the ring plane.

#### 3.2. $S_0$ -min structure

In the current work, we considered the *trans*-nitrofuranoin given in Scheme 2, because this configuration is the stable isomer in the drug crystal(Bandoli et al., 2013). The  $S_0$  minimum-energy geometry ( $S_0$ -min) of *trans*-nitrofuranoin optimized at the DFT-B3LYP/6-31G\* level is shown in Fig. S2(a) in SI. The backbone of  $S_0$ -min is planar and the  $C_a-N_a$  bond ( $r_a$ ) length considered is 1.429 Å.

At  $S_0$ -min, the excited-state properties, including the transition energies, the dipole moments, the oscillator strengths and the dominant electronic transitions, were calculated at the SA(6)-CASSCF(16,11)/6-31G\* and MS(6)-CASPT2(16,11)/6-31G\* levels, as given in Table S1 in SI. All involved molecular orbitals are given in Fig. 1. Both SA-CASSCF and MS-CASPT2 calculations give rather consistent results on the first two excited states, which predict that  $S_1$  and  $S_2$  states are essentially dark with vanishing oscillator strengths. The first excited state  $S_1$  (SA-CASSCF: 3.66 eV and MS-CASPT2: 3.71 eV) displays the ( $n_2\pi_1^*$ ) character. The  $n_2$  orbital here is located at the  $NO_2$  group, while the  $\pi_1^*$  orbital



**Scheme 2.** Molecular structure and atomic labels of *trans*-nitrofuranoin.

**Table 1**  
Important internal coordinates.

Label	Internal Coordinates	Motion
$r_a$	distance $C_a-N_a$	stretching of $C_a-N_a$ bond
$r_b$	distance $N_a-O_a$	stretching of $N_a-O_a$ bond
$r_c$	distance $N_a-O_b$	stretching of $N_a-O_b$ bond
$\theta_a$	angle $O_a-N_a-O_b$	expansion or contraction of the angle
$\tau_a$	dihedral angle $C_b-C_a-N_a-O_a$	internal rotation of $NO_2$ group
$\tau_b$	dihedral angle $O_c-C_a-N_a-O_b$	internal rotation of $NO_2$ group
$\tau_c$	dihedral angle $C_d-C_e-N_b-N_c$	torsion along with the central $C_eN_b$ bond
$\tau_d$	dihedral angle $C_d-N_b-H_a-C_e$	pyramidalization at the $C_e$ atom
$\tau_e$	dihedral angle $C_a-O_a-O_b-N_a$	pyramidalization at the $N_a$ atom
$\tau_f$	dihedral angle $C_b-O_c-C_a-N_a$	out-of-plane motion of the $NO_2$ group

(LUMO) is located at both the  $NO_2$  group and the central CN bond. The second excited state  $S_2$  (CASSCF: 4.27 eV and MS-CASPT2: 4.29 eV) is mainly attributed as the ( $n_1\pi_1^*$ ) character. The  $n_1$  orbital is also located at the  $NO_2$  group. In fact, the above  $n_1$  orbital and  $n_2$  orbital can be viewed as the symmetric and antisymmetric combination of two localized n orbitals of the  $NO_2$  group. At the same time, the minor double excitation characters also exist for the  $S_2$  state.

The SA-CASSCF and MS-CASPT2 calculations predict different transition properties for the  $S_3$  and  $S_4$  states. The  $S_3$  state (5.51 eV) is a dark  $\pi\pi^*$  state at the SA-CASSCF level, while the same transition gives the  $S_4$  state (5.59 eV) at the MS-CASPT2 level. The bright  $\pi\pi^*$  (HOMO-LUMO) state is the  $S_4$  state (5.72 eV) at the CASSCF level, while the same electronic character is dominant at the  $S_3$  state (4.41 eV) at the MS-CASPT2 level. At the MS-CASPT2 level, the permanent dipole moments of three lowest excited states ( $S_1$ : 5.36 Debye;  $S_2$ : 5.44 Debye;  $S_3$ : 5.46 Debye) are smaller than that of the  $S_4$  state (7.85 Debye), indicating the charge transfer character of the  $S_4$  state.

For benchmark, we performed the geometry optimization of  $S_0$ -min at the DFT-CAM-B3LYP/6-31+G(d,p) and DFT-M06-2X/6-31+G(d,p) levels. The excited states at these new optimized geometries were calculated at MS(6)-CASPT2(16,11)/6-31G\* level. The geometries of these new  $S_0$ -min are very similar to the one optimized at the DFT-B3LYP/6-31G\* level. The excitation energies of excited states are also consistent at these minima, except small differences for the high-lying excited states, while such minor deviation is acceptable considering the accuracy of the excited state calculations. All results were shown in the Figs. S2(b–c) and Table S2 in the SI.

We also obtained the  $S_1$  minimum (labelled as  $S_1$ -min) and all informations were given in SI.

### 3.3. Preliminary understanding of nonadiabatic dynamics

To obtain the first view on the possible photoinduced reaction channels, we first ran the preliminary nonadiabatic dynamics with low computational cost to obtain a rough understanding of the nonadiabatic

dynamics. As discussed above, several initial conditions with different velocities and different initial states were taken in the TSH dynamics.

We collected all TSH trajectories and then noticed that several different types of them were obtained. First, some trajectories show the direct cleavage of the NO bond of the  $NO_2$  group. For all trajectories following this NO bond cleavage channel, the time-dependent PESs become degenerated with the NO bond breaking. We observed that when the NO bond distance ( $r_b$  or  $r_c$ ) is longer than 2.22 Å, the  $S_1-S_0$  energy gap is less than 0.02 eV. In the same time, the non-breaking NO bond displays a strong out-of-plane motion with respect to the ring plane. The dissociation limit displays the multi-reference characters and three lowest electronic states become completely degenerated. A typical trajectory is given in Fig. S5 in SI.

Second, by analyzed the geometrical features of all  $S_1-S_0$  hopping geometries collected from the TSH dynamics of all initial conditions, several internal conversion channels were identified, which should pass different  $S_0/S_1$  CIs.

The first group of trajectories experiencing the internal conversion dynamics display the torsional motion of the central  $C_eN_b$  bond. For other trajectories, we observed that all hopping geometries are characterized by the different motions of the  $NO_2$  group, while the five-member ring containing  $N_c$  atom does not give the large geometry deformation. In order to fully understand the features of the geometries, the classical MDS analysis was used to visualize the geometry distribution of hops in the reduced two-dimensional space and the details of this method can be found in previous work (Li et al., 2017, 2018). In the results, for all non-isomerizaton hops, several geometry deformation features exist, for instance the torsional motion of the  $NO_2$  group along the  $C_aN_a$  bond, the pyramidalization of the  $N_a$  atom, the out-of-plane motion of the  $NO_2$  group and the pyramidalization motion at the  $C_a$  atom of the five-membered ring part. Some hopping geometries display the mixture of these motion. In addition, some hopping geometries show the rather flat geometry in the  $NO_2$  group part. In order to identify of the key internal coordinates responsible for the excited-state dynamics, we tried to optimized the  $S_0/S_1$  CIs from the typical geometries of these hopping geometries. All details of analysis of the hopping geometries and the way to choose the typical geometries are given in SI.

### 3.4. Conical intersections

To know which  $S_0/S_1$  CIs are responsible for the decay dynamics of nitrofurantoin, we optimized the  $S_0/S_1$  CIs from hopping geometries at the SA(3)-CASSCF(16,11)/6-31G\* level and then three  $S_0/S_1$  CIs were located. All correspondence between hopping geometries and CIs are shown in the Table S4 in SI.

Starting from the hopping geometries with the  $C_eN_b$  bond isomerization, the first  $S_0/S_1$  CI (CI<sub>01</sub>-I in Fig. 2(a)) is located successfully and it is sufficiently characterized by the dihedral angle  $\tau_c = 108.2^\circ$ . Besides the twisting motion, the elongation of the central  $C_eN_b$  bond (~1.355 Å) and pyramidalization motion at the  $C_e$  atom ( $\tau_d=11.4^\circ$ ) is also observed at the CI<sub>01</sub>-I geometry. This clearly indicates that the existence of the

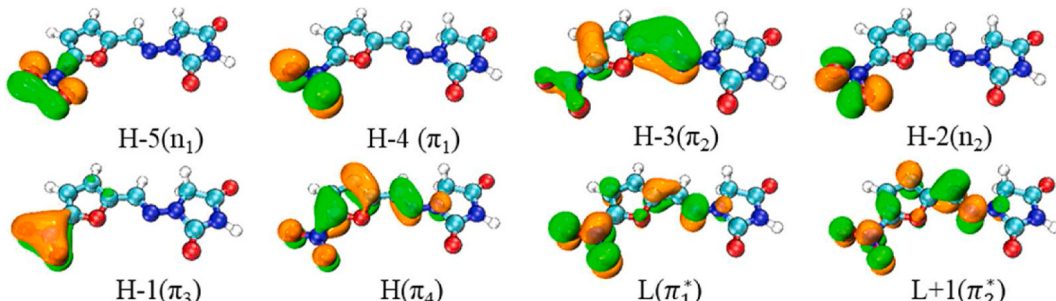


**Fig. 1.** Some frontier molecular orbitals at  $S_0$ -min of *trans*-nitrofurantoin. The labels "H" and "L" represent HOMO and LUMO, respectively. Here the results are from the SA(6)-CASSCF(16,11)/6-31G\* calculations.

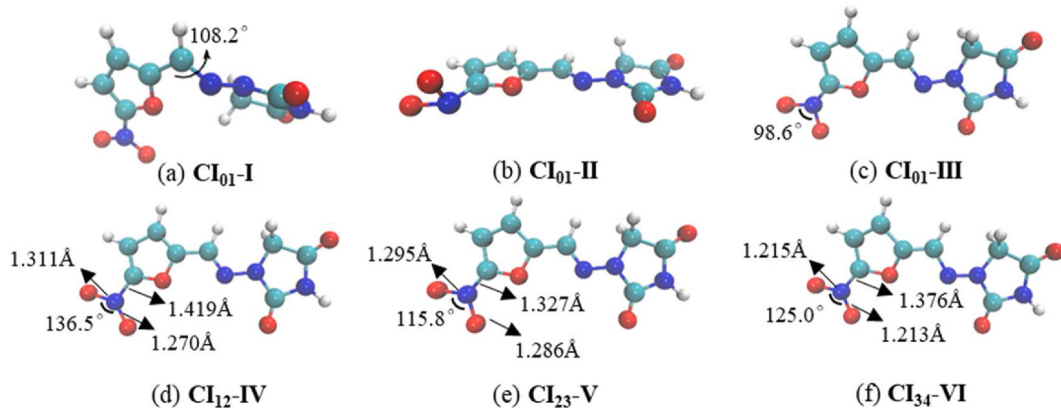


**Fig. 2.** (a)–(c) The S<sub>0</sub>/S<sub>1</sub> Cls optimized at the SA(3)-CASSCF(16,11)/6-31G\* level; (d) The S<sub>1</sub>/S<sub>2</sub> CI optimized at the SA(4)-CASSCF(16,11)/6-31G\* level; (e) The S<sub>2</sub>/S<sub>3</sub> CI optimized at the SA(6)-CASSCF(16,11)/6-31G\* level; (f) The S<sub>3</sub>/S<sub>4</sub> CI optimized at the SA(6)-CASSCF(16,11)/6-31G\* level.

photoisomerization channel in the nonadiabatic dynamics of nitrofurantoin. As shown in Fig. S9(a) in SI, the degenerated S<sub>0</sub>/S<sub>1</sub> wave functions at the Cl<sub>01</sub>-I display the strong mixture between the closed-shell and the  $\pi\pi^*$  electronic characters. This  $\pi\pi^*$  character at the Cl<sub>01</sub>-I corresponds to the bright electronic state at the FC region.

Starting from the non-isomerization hopping geometries, the optimization of S<sub>0</sub>/S<sub>1</sub> CI results in two different Cls, Cl<sub>01</sub>-II and Cl<sub>01</sub>-III (see Fig. 2(b) and (c)), and both do not show any isomerization motion of the C<sub>e</sub>N<sub>b</sub> bond.

At Cl<sub>01</sub>-II, the dihedral angles of  $\tau_a$ ,  $\tau_b$  and  $\tau_e$  are 9.9, 90.0 and 34.0°, respectively. It is obvious that the main geometrical features of the Cl<sub>01</sub>-II are characterized by the internal rotational motion of the NO<sub>2</sub> group along the C<sub>a</sub>N<sub>a</sub> bond and the pyramidalization motion at the N<sub>a</sub> atom. Starting from the Cl<sub>01</sub>-II, the rigorous scan indicates that the S<sub>1</sub>-S<sub>0</sub> energy gap remains very small with the torsional motion of the NO<sub>2</sub> group along the C<sub>a</sub>N<sub>a</sub> bond (see Fig. S10 in SI). This can well explain why many hopping geometries display the significant pyramidalization motion at the N<sub>a</sub> atom, while the rotational orientations of the NO<sub>2</sub> group along the C<sub>a</sub>N<sub>a</sub> bond are different. The electronic transitions in the lowest doubly degenerated electronic states at the Cl<sub>01</sub>-II are composed of several components. Several frontier orbitals involving in the electronic transitions display the significant n/π orbitals mixture, and thus this CI displays the (close-shell/nπ<sup>\*</sup>/ππ<sup>\*</sup>) mixing character, as shown in Fig. S9(b) in SI.

The third S<sub>0</sub>/S<sub>1</sub> CI (Cl<sub>01</sub>-III) does not show the obvious ring and backbone deformation. With respect to the S<sub>0</sub>-min, the most significant geometrical difference is that the  $\theta_a$  angle becomes much smaller ( $\theta_a=98.6^\circ$ ) at the Cl<sub>01</sub>-III. At the same time, the C<sub>a</sub>N<sub>a</sub> bond length decreases to only 1.274 Å. The electronic transition components of the two lowest electronic states display the close-shell/nπ<sup>\*</sup> mixture (shown in Fig. S9(c) in SI). Possibly due to the small geometry deformation, the nπ<sup>\*</sup> state corresponds to the S<sub>1</sub> state at the S<sub>0</sub>-min. Besides, the dipole moments of the two lowest states (S<sub>0</sub> and S<sub>1</sub>) of all S<sub>0</sub>/S<sub>1</sub> Cls are given in the Table S5 in the SI. At Cl<sub>01</sub>-II and Cl<sub>01</sub>-III, the S<sub>0</sub> and S<sub>1</sub> states show the large dipole moments, possibly due to their charge transfer characters caused by the weak overlap of the electronic orbitals involved in the transitions.

In addition, Fig. 2(d)~(f) show the S<sub>1</sub>/S<sub>2</sub>, S<sub>2</sub>/S<sub>3</sub>, S<sub>3</sub>/S<sub>4</sub> Cls, respectively. Their geometries do not show the large geometry deformation with respect to the S<sub>0</sub>-min, while some differences exist in the  $\theta_a$  angle. This indicates that the lower electronic states may be accessed via these Cls in principle. We expected that the S<sub>1</sub> states should be easily accessed in the early time of the photo-induced dynamics, even if in principle the dynamics starts from a higher bright electronic state. Afterward, the excited-state dynamics should mainly take place on the S<sub>1</sub> state. As expect, the high kinetic energy released from the decay dynamics from the higher electronic states should results in the opening of more

reaction channels that does not appear in the low-energy initial conditions.

We show the energy levels of electronic states of all important geometries including S<sub>0</sub>-min, S<sub>1</sub>-min, Cl<sub>01</sub>-I, Cl<sub>01</sub>-II, Cl<sub>01</sub>-III, Cl<sub>12</sub>-IV, Cl<sub>23</sub>-V and Cl<sub>34</sub>-VI in Fig. 3. At the SA(6)-CASSCF(16,11)/6-31G\* and MS(6)-CASSCF(16,11)/6-31G\* levels, all CI optimized by using different state-averaged calculations show the small energy gaps between two relevant electronic states, which means their geometries are reasonable. In particular, due to the non-convergent and unreasonable results in the other optimization level (see discussion in Fig. S11 in SI), we only show the S<sub>1</sub>/S<sub>2</sub> CI geometry obtained at the SA(4)-CASSCF(16,11)/6-31G\*. The energy of S<sub>1</sub> state of two S<sub>0</sub>/S<sub>1</sub> Cls (Cl<sub>01</sub>-I and Cl<sub>01</sub>-III) lies below that it at the S<sub>0</sub>-min at both the SA-CASSCF and MS-CASPT2 levels. As the contrast, the SA-CASSCF calculations show that the energy of Cl<sub>01</sub>-II is lower than the S<sub>1</sub> state at the S<sub>0</sub>-min, while the MS-CASPT2 calculations show the reversed results. This indicates that such a channel may be suppressed at the MS-CASPT2 level.

### 3.5. Reaction pathways

To understand the reaction path of all channels, we performed the linear interpolated excited-state pathways from the S<sub>0</sub>-min to each optimized CI.

For the NO bond cleavage channel, we simply enlarged the NO bond distance and built the PES. The SA(6)-MS-CASPT2(16,11)/6-31G\* and SA(6)-CASSCF(16,11)/6-31G\* methods were employed to build the relevant potential energy surfaces. In fact, two such channels, namely Channel-1- $\alpha$  and Channel-1- $\beta$ , should exist due to the existence of two O atoms in NO<sub>2</sub> groups shown in Fig. 4(a) and (b). When the NO bond breaks, three lowest states (S<sub>0</sub>-S<sub>2</sub>) become completely degenerated and the same happens for S<sub>3</sub>-S<sub>5</sub>. This indicates that the electronic states acquire multi-reference characters at the dissociation limit. The reason is very simple. The photoproduct here contains the O atom. Four electrons are distributed in three p orbitals for this O atom, giving three degenerated electronic configurations and three lowest electronic states become degenerated. This dissociation limit is certainly accessible if the dynamics starts from higher electronic states.

The PESs in Fig. 4(c) shows the reaction pathways of the photo-induced isomerization channel, namely from the S<sub>0</sub>-min to Cl<sub>01</sub>-I. At the SA-CASSCF level, the bright state is S<sub>4</sub> state at the FC region and the S<sub>1</sub>-S<sub>3</sub> states are dark states. At the MS-CASPT2 level, the S<sub>3</sub> state is bright state and the S<sub>1</sub>-S<sub>2</sub> states are dark states. The  $\pi\pi^*$  electronic configuration, which as same as the electronic wave functions of the S<sub>0</sub> and S<sub>1</sub> states displayed in Cl<sub>01</sub>-I, appears on the S<sub>4</sub> state (SA-CASSCF) or S<sub>3</sub> state (MS-CASPT2) in the FC region. This indicates that the energy of the  $\pi\pi^*$  electronic configuration should become lower along the C<sub>e</sub>N<sub>b</sub> bond twisting motion, which finally interacts with the closed-shell component

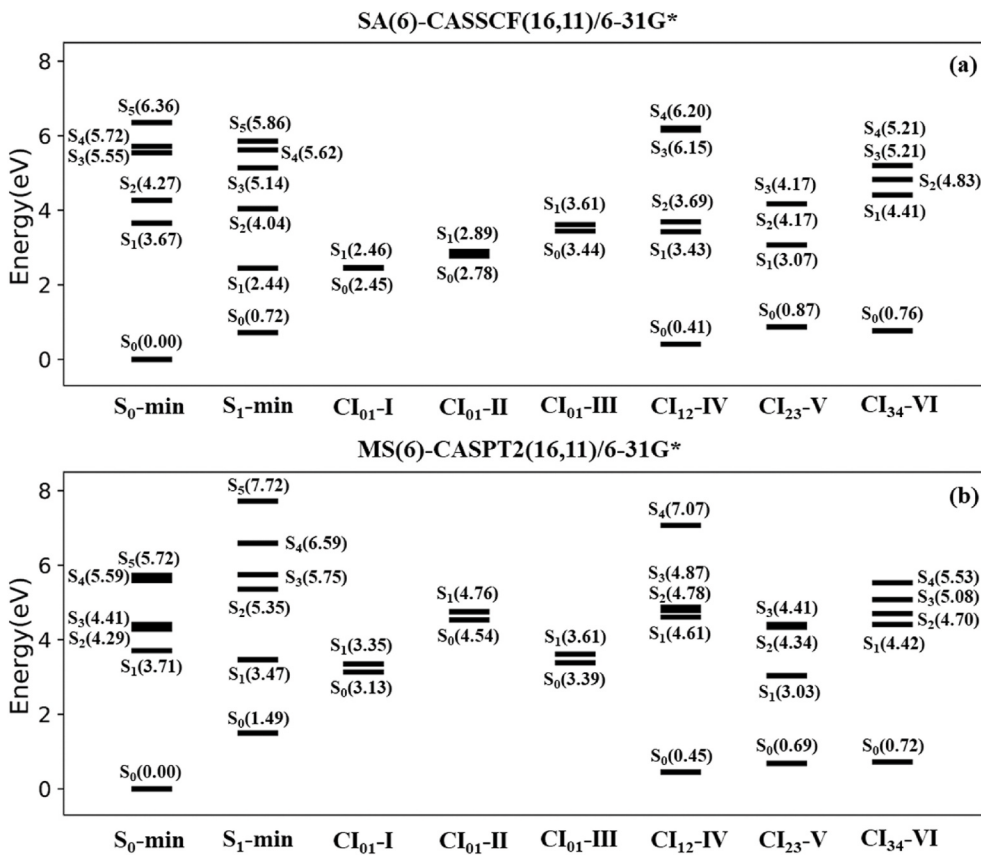


**Fig. 3.** The energy level diagram of electronic states at important geometries including  $S_0$ -min,  $S_1$ -min,  $CI_{01}$ -I,  $CI_{01}$ -II,  $CI_{01}$ -III,  $CI_{12}$ -IV,  $CI_{23}$ -V and  $CI_{34}$ -VI.

to create the  $CI_{01}$ -I. Also considering the existence of several excited-state CIs, it is rather clearly that the isomerization channel should exist from the FC region to the  $CI_{01}$ -I in Fig. 4(c). This isomerization channel opens the possibility to form the *cis*-isomer. This well explains the experimental result that the *cis*-isomer product is observed in the photochemistry of nitrofuranoin (Edlund et al., 2006).

The PESs from  $S_0$ -min to the  $CI_{01}$ -II (characterized by the strong pyramidalization at the  $N_a$  atom and the internal rotation of the  $NO_2$  group) are given in Fig. 4(d). At the SA-CASSCF level, this  $CI_{01}$ -II lies lower than the  $S_1$  state at the FC region. This means that the  $CI_{01}$ -II can be accessed in the photo-induced dynamics of nitrofuranoin, even if the dynamics starts from the  $S_1$  state. The same  $CI_{01}$ -II shows much higher energy at the MS-CASPT2 level. Because the  $S_3$  state becomes bright in the MS-CASPT2 level, it looks that this channel may not be easily accessible from the bright  $S_3$  state. In this sense, for this particular channel, the SA-CASSCF and MS-CASPT2 calculations may predict different possibility.

The channel from  $S_0$ -min to the  $CI_{01}$ -III mainly displays the bending motion of the  $NO_2$  group. We label this channel as Channel-4 and the PESs are shown in Fig. 4(e). At the SA-CASSCF level, the  $CI_{01}$ -III geometry does not show the strong geometry distortion with respect to the  $S_0$ -min, and thus the electronic character of the  $S_1$  state remains unchanged in this channel. The reaction pathway from  $S_0$ -min to  $CI_{01}$ -III is barrierless on the  $S_1$  state at both SA-CASSCF and MS-CASPT2 level. This channel should also be accessible to the photo-induced reactions of nitrofuranoin.

### 3.6. Discussions

Here we wish to provide some general discussions on the current theoretical description of the photochemistry of nitrofuranoin.

In this work, we first used the TSH dynamics to get reaction channels

on the photo-induced reactions. Because this step is only used for the identification of the possibly involved  $S_0/S_1$  CIs, we took the SA-CASSCF level with a small active space CAS(12,9) and a rather low basis set 6-31G. This setup allows us to run the TSH dynamics with a reasonable computational cost. If we use more accurate setups here, for instance, using the 6-31G\* basis set, the TSH dynamics calculations become much slower. Since the hopping geometries were taken as the initial guess to perform the CI optimization, this setup is acceptable.

In the second step of the CI optimization, we took a larger active space CAS(16,11) and a reasonable basis set 6-31G\*, while only three relevant electronic states were taken into account in the state-averaged calculations. However, in some cases, we found that it is necessary to include a higher electronic state to get the more reasonable results when the higher state is close to the  $S_1$  state during the optimization. But the inclusion of too many electronic states in the SA-CASSCF calculations may cause the convergence problems in the CI optimization. Considering all above issues, we chose the current setup to balance the computational cost, efficiency and convergence. The results show the current setups give the proper CI geometries, because the energy gaps at the CIs remain very small in the PES calculations at the SA(6)-CASSCF and MS(6)-CASPT2 levels.

Since the photo-absorption generates a high-lying bright state, the initial energy should be rather high, which may have a deep impact on the further dynamics. Here we mainly assume that the dynamics finally goes to the  $S_1$  states and the system decays via the  $S_0/S_1$  CI, or accesses the O atom dissociation limit with state degeneracy. This means that the current approaches cannot describe the direct excited-state photolysis channels that does not involve the  $S_0$  state at all. This is the limitation of the current approaches. However, such types of channels should play a rather minor role here. Our calculations clearly show the presents of several excited-state CIs, which should be easily accessed by the molecular vibrations. Particularly due to the large size of the current

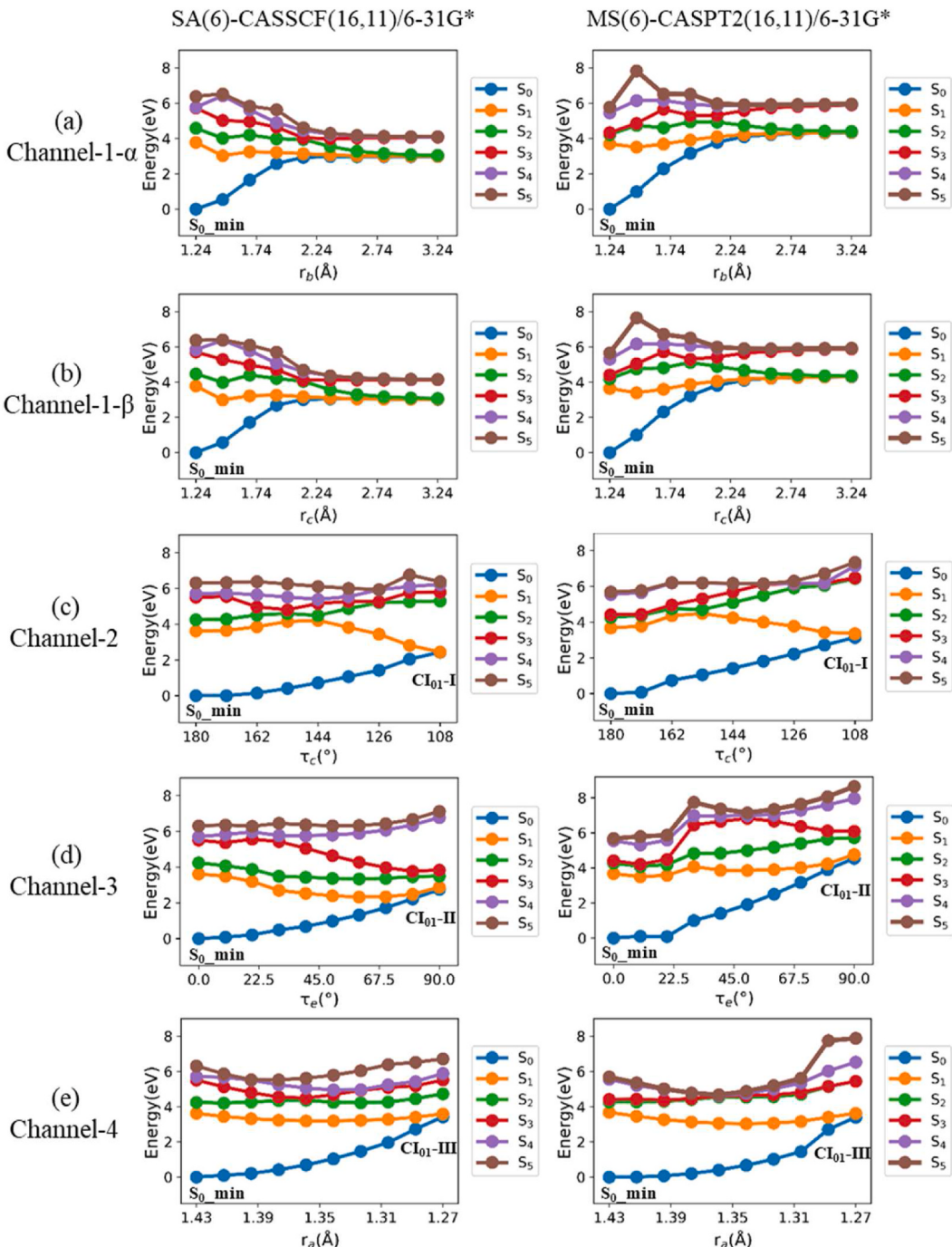


**Fig. 4.** Linear-interpolated excited-state pathways at both SA-CASSCF and MS-CASPT2 levels. (a) Channel-1- $\alpha$  and (b) Channel-1- $\beta$  show the  $\text{N}_2\text{O}_2$  bond and  $\text{N}_2\text{O}_2$  bond cleavage channels, respectively; (c), (d) and (e) give the photo-induced isomerization channel (Channel-2), the  $\text{N}_2$ -pyramidalization channel (Channel-3) and  $\text{NO}_2$  group contraction channel (Channel-4), respectively.

system, the vibrational relaxation damps the additional energy after the internal conversion dynamics to the lower excited state. As a result, the lowest  $S_1$  electronic state may be easily reached for the current system. This argument is highly consistent with the famous Kasha rule (Kasha, 1950; Klán and Wirz, 2009). However, when the  $S_1$  state is reached, the kinetic energy of the system must be high. To mimic this case, we considered running TSH dynamics under the initial conditions with large velocity. This way helps us to get more possible decay channels.

Although various electronic structure methods, such as TDDFT, SA-CASSCF, MS-CASPT2 and so on, were developed for the excited-state calculations of the excited states, it is necessary to select the

reasonable approaches to avoid their individual limitations. In our work, one of the critical issues is whether it is suitable to use the single-reference theories (such as TDDFT) in the TSH and PES calculations. These black-box theories require much less computational cost. However, it is not suitable to use these single-reference methods to treat the current problem. We noticed that the O-atom detachment channel displays the highly degenerated dissociation limit. In this case, the ground state shows multi-reference electronic characters that cannot be well captured by the single-reference theories. For this reason, it is necessary to use the multi-reference methods such as SA-CASSCF and MS-CASPT2. As noticed, there is a visible discrepancy between MS-

CASPT2 and SA-CASSCF results for the third channel. One of the possible reason is that the SA-CASSCF does not include dynamical electronic correlations for the inactive orbitals, whereas the MS-CASSPT2 considers such effect only by the second-order perturbation. Thus it is quite normal that they give different results. In fact, this represents one of most key challenges in the research field of excited-state quantum chemistry. It is generally assumed that the MS-CASPT2 method is more accurate than the SA-CASSCF method, although the MS-CASPT2 method itself suffers from many deficiencies. However, the current work gives the rather preliminary discussions on the possible excited-state channels on such large compound. We wish that this work will invoke the further experimental and theoretical works to examine all mechanisms in details. In this sense, this discrepancy should does not cause major problem here.

#### 4. Conclusions

In this work, we combined the on-the-fly Tully's TSH dynamics, CI optimizations and excited-state pathway calculations to study the photochemistry of the *trans*-isomer of nitrofurantoin, which is a widely-used drug compound potentially harmful to environments. The preliminary TSH calculations with different initial conditions were run to examine the nonadiabatic dynamics, giving the photolysis and internal conversion channels. All  $S_1-S_0$  hopping geometries were examined to identify the possible reaction channels responsible for the internal conversion to the ground state. In this step, two unsupervised machine learning approaches, namely the dimensionality reduction and clustering approaches, were employed in the analysis. Next, starting from the  $S_1-S_0$  hopping geometries, the CI optimizations were performed. Finally, the reaction pathways from the FC region to these CIs were built to provided the possible photo-induced reaction channels of nitrofurantoin clearly.

The current calculations totally found four possible reaction channels in the photochemistry of nitrofurantoin. The first channel (Channel-1) is the photolysis channel, in which one of the NO bonds of the  $\text{NO}_2$  group breaks and the dissociation limit displays the multi-reference characters due to the existence of highly degenerated states. The second channel (Channel-2) corresponds to the strong isomerization of the central CN bond. The third channel (Channel-3) are characterized by the pyramidalization at the N atom of  $\text{NO}_2$  group and the internal rotation of  $\text{NO}_2$  with respect to the CN bond. The fourth channel (Channel-4) is governed by the bending motion of the ONO angle in the  $\text{NO}_2$  group. Channel-2, 3 and 4 result in the internal conversion dynamics to the ground states. For most channels, the SA-CASSCF and MS-CASPT2 calculations give rather consistent results. Only for the third channel relevant to the internal rotation motion of  $\text{NO}_2$  group, the MS-CASPT2 calculations indicate that the  $S_0/S_1$  CI lies in a high energy domain, implying that this channel is not easy to be reached, while the contrast conclusion was made at the SA-CASSCF level. Considering the bright state is high in energy and the CIs exist between excited states, Channel 1–4 may be relevant to the photo-induced dynamics of nitrofurantoin.

The current approach represents our first effort towards the understanding of the photochemistry of nitrofurantoin-family compounds, and provide some hints on the photo-induced reactions of nitrofurantoin such as the photo-isomerization channel, which clearly explain some key features in the experimental observations(Edhlund et al., 2006; Szabó-Bárdos et al., 2020). However, additional efforts should be conducted in the theoretical studies of the photochemistry of the current systems. It should be interesting to check the solvent effects on the nonadiabatic dynamics. And besides, due to the strong deformation of  $\text{NO}_2$  group in the photo-induced excited state reactions in our current results, it also suggest us that the existence of the hydrogen bonds in the aqueous solutions may have the potential impacts on these channels. The simulation on the role of water molecules in the excited-state dynamics of nitrofurantoin may provide some ideas on why the rearrangement of the  $\text{NO}_2$  group was observed in the photoreactions

(Edhlund et al., 2006). Additionally, the study on the possible involvement of the triplet states may also be rather interesting(Szabó-Bárdos et al., 2020). All of them should be challenging topics in further studies. In addition, the on-the-fly nonadiabatic dynamics(Cattaneo and Persico, 2001; Ben-Nun and Martínez, 2002; Domcke et al., 2004, 2011; Barbatti et al., 2007; Fabiano et al., 2008; Lan et al., 2009; Barbatti, 2011; Richter et al., 2011; Wohlgemuth et al., 2011; Johnson and Martínez, 2012; Du and Lan, 2015a, 2015b; Curchod and Martínez, 2018; Mai et al., 2018; Persico and Granucci, 2018; Xu et al., 2018) and excited-state pathway construction(Domcke et al., 2004, 2011) are very important tool in the study of photochemistry of polyatomic systems in recent years. We believe that these tools will play more and more important simulation roles in the exploration of environmental photochemistry in the future.

#### Credit author statement

Kunni Lin: Conceptualization, Methodology, Formal analysis, Investigation, Writing – original draft, Visualization. Deping Hu: Formal analysis, Investigation, Visualization. Jiawei Peng: Formal analysis, Visualization. Chao Xu: Formal analysis, Writing – original draft. Feng Long Gu: Supervision, Project administration, Funding acquisition. Zhenggang Lan: Conceptualization, Writing – original draft, Formal analysis, Supervision, Project administration, Funding acquisition

#### Declaration of competing interest

The authors declare that they have no known competing financial interests or personal relationships that could have appeared to influence the work reported in this paper.

#### Acknowledgments

This work is supported by the National Key R&D Program of China (Grant No. 2017YFB0203403), the NSFC projects (No. 21873112, 21933011) and the Guangdong Youth Innovative Talents and Natural Science Foundation of Guangdong Province (Grant 2018A030310660).

#### Appendix A. Supplementary data

Supplementary data to this article can be found online at <https://doi.org/10.1016/j.chemosphere.2021.130831>.

#### References

- Aguilera-Porta, N., Corral, I., Muñoz-Muriedas, J., Granucci, G., 2019. Excited state dynamics of some nonsteroidal anti-inflammatory drugs: a surface-hopping investigation. *Comput. Theor. Chem.* 1152, 20–27.
- Albini, A., Fasani, E., 2007. Drugs: Photochemistry and Photostability. Royal Society of Chemistry.
- Andersson, K., Malmqvist, P.Å., Roos, B.O., Sadlej, A.J., Wolinski, K., 1990. Second-order perturbation theory with a CASSCF reference function. *J. Phys. Chem.* 94, 5483–5488.
- Andersson, K., Malmqvist, P.Å., Roos, B.O., 1992. Second-order perturbation theory with a complete active space self-consistent field reference function. *J. Chem. Phys.* 96, 1218–1226.
- Aquilante, F., Autschbach, J., Baiardi, A., Battaglia, S., Borin, V.A., Chibotaru, L.F., Conti, I., De Vico, L., Delcey, M., Galván, F., I. Ferré, N., Freitag, L., Garavelli, M., Gong, X., Knecht, S., Larsson, E.D., Lindh, R., Lundberg, M., Malmqvist, P.Å., Nenov, A., Norell, J., Odelius, M., Olivucci, M., Pedersen, T.B., Pedraza-González, L., Phung, Q.M., Pierloot, K., Reiher, M., Schapiro, I., Segarra-Martí, J., Segatta, F., Seijo, L., Sen, S., Sergentu, D.C., Stein, C.J., Ungur, L., Vacher, M., Valentini, A., Veryazov, V., 2020. Modern quantum chemistry with [Open]Molcas. *J. Chem. Phys.* 152, 214117.
- Bahnemann, D.W., Robertson, P.K., 2015. Environmental Photochemistry Part III. Springer.
- Bailey, R.R., Gower, P.E., Roberts, A.P., De Wardener, H.E., 1971. Prevention of urinary-tract infection with low-dose nitrofurantoin. *Lancet* 298, 1112–1114.
- Bandoli, G., Ongaro, A., Lotto, F., Rossi, M., 2013. Crystal data of nitrofurantoin C8H16N4O5. *Powder Diffr.* 8, 107–108.
- Barbatti, M., 2011. Nonadiabatic dynamics with trajectory surface hopping method. *Wires. Comput. Mol. Sci.* 1, 620–633.

- Barbatti, M., Granucci, G., Persico, M., Ruckenbauer, M., Vazdar, M., Eckert-Maksić, M., Lischka, H., 2007. The on-the-fly surface-hopping program system Newton-X: application to ab initio simulation of the nonadiabatic photodynamics of benchmark systems. *J. Photochem. Photobiol. A* 190, 228–240.
- Ben-Nun, M., Martínez, T.J., 2002. Ab initio quantum molecular dynamics. *Adv. Chem. Phys.* 121, 439–512.
- Borg, I., Groenen, P., 2005. Modern Multidimensional Scaling Theory and Applications. Springer Science & Business Media.
- Boule, P., 2013. Environmental Photochemistry. Springer, Berlin Heidelberg.
- Cattaneo, P., Persico, M., 2001. Semiclassical simulations of azomethane photochemistry in the gas phase and in solution. *J. Am. Chem. Soc.* 123, 7638–7645.
- Challis, J.K., Carlson, J.C., Friesen, K.J., Hanson, M.L., Wong, C.S., 2013. Aquatic photochemistry of the sulfonamide antibiotic sulfapyridine. *J. Photochem. Photobiol. A* 262, 14–21.
- Chen, Y., Hu, C., Qu, J., Yang, M., 2008. Photodegradation of tetracycline and formation of reactive oxygen species in aqueous tetracycline solution under simulated sunlight irradiation. *J. Photochem. Photobiol. A* 197, 81–87.
- Chen, Z.F., Ying, G.G., Jiang, Y.X., Yang, B., Lai, H.J., Liu, Y.S., Pan, C.G., Peng, F.Q., 2014. Photodegradation of the azole fungicide fluconazole in aqueous solution under UV-254: kinetics, mechanistic investigations and toxicity evaluation. *Water Res.* 52, 83–91.
- Curchod, B.F.E., Martínez, T.J., 2018. Ab initio nonadiabatic quantum molecular dynamics. *Chem. Rev.* 118, 3305–3336.
- De Silva, V., Tenenbaum, J.B., 2004. Sparse Multidimensional Scaling Using Landmark Points. Technical Report. Stanford University.
- Domecke, W., Yarkony, D.R., Köppel, H., 2004. Conical Intersections I: Electronic Structure, Dynamics and Spectroscopy. World Scientific, Singapore.
- Domecke, W., Yarkony, D.R., Köppel, H., 2011. Conical Intersections II: Theory, Computation and Experiment. World Scientific, Singapore.
- Du, L., Lan, Z., 2015a. Correction to "an on-the-fly surface-hopping program JADE for nonadiabatic molecular dynamics of polyatomic systems: implementation and applications". *J. Chem. Theor. Comput.* 11, 4522–4523.
- Du, L., Lan, Z., 2015b. An on-the-fly surface-hopping program JADE for nonadiabatic molecular dynamics of polyatomic systems: implementation and applications. *J. Chem. Theor. Comput.* 11, 1360–1374.
- Ehdlund, B.L., Arnold, W.A., McNeill, K., 2006. Aquatic photochemistry of nitrofuran antibiotics. *Environ. Sci. Technol.* 40, 5422–5427.
- Fabiano, E., Keal, T.W., Thiel, W., 2008. Implementation of surface hopping molecular dynamics using semiempirical methods. *Chem. Phys.* 349, 334–347.
- Frisch, M.J., Trucks, G.W., Schlegel, H.B., Scuseria, G.E., Robb, M.A., Cheeseman, J.R., Scalmani, G., Barone, V., Petersson, G.A., Nakatsuji, H., Li, X., Caricato, M., Marenich, A.V., Bloino, J., Janesko, B.G., Gomperts, R., Mennucci, B., Hratchian, H.P., Ortiz, J.V., Izmaylov, A.F., Sonnenberg, J.L., Williams Ding, F., Lipparini, F., Egidi, F., Goings, J., Peng, B., Petrone, A., Henderson, T., Ranasinghe, D., Zákřezkova, V.G., Gao, J., Rega, N., Zheng, G., Liang, W., Hada, M., Ehara, M., Toyota, K., Fukuda, R., Hasegawa, J., Ishida, M., Nakajima, T., Honda, Y., Kitao, O., Nakai, H., Vreven, T., Throssell, K., Montgomery Jr., J.A., Peralta, J.E., Ogliaro, F., Bearpark, M.J., Heyd, J.J., Brothers, E.N., Kudin, K.N., Staroverov, V.N., Keith, T.A., Kobayashi, R., Normand, J., Raghavachari, K., Rendell, A.P., Burant, J.C., Iyengar, S.S., Tomasi, J., Cossi, M., Millam, J.M., Klene, M., Adamo, C., Cammi, R., Ochterski, J.W., Martin, R.L., Morokuma, K., Farkas, O., Foresman, J.B., Fox, D.J., 2016. Gaussian 16. Rev. C.01, Wallingford, CT.
- Galván, F., I., Vacher, M., Alavi, A., Angel, C., Aquilante, F., Autschbach, J., Bao, J.J., Bokarev, S.I., Bogdanov, N.A., Carlson, R.K., Chibotaru, L.F., Creutzberg, J., Dattani, N., Delcay, M.G., Dong, S.S., Drew, A., Freitag, L., Frutos, L.M., Gagliardi, L., Gendron, F., Giussani, A., González, L., Grell, G., Guo, M., Hoyer, C.E., Johansson, M., Keller, S., Knecht, S., Kovacević, G., Källman, E., Li Manni, G., Lundberg, M., Ma, Y., Mai, S., Malhado, J.P., Malmqvist, P.Å., Marquetand, P., Mewes, S.A., Norell, J., Olivucci, M., Oppel, M., Phung, Q.M., Pierloot, K., Plasser, F., Reiher, M., Sand, A.M., Schapiro, I., Sharma, P., Stein, C.J., Sørensen, L.K., Truhlar, D.G., Ugand, M., Ungur, L., Valentini, A., Vancollie, S., Veryazov, V., Weser, O., Wesolowski, T.A., Widmark, P.-O., Wouters, S., Zech, A., Zobel, J.P., Lindh, R., 2019. OpenMolcas: from source code to insight. *J. Chem. Theor. Comput.* 15, 5925–5964.
- García-Galán, M.J., Díaz-Cruz, M.S., Barceló, D., 2012. Kinetic studies and characterization of photolytic products of sulfamethazine, sulfapyridine and their acetylated metabolites in water under simulated solar irradiation. *Water Res.* 46, 711–722.
- Ge, L., Chen, J., Wei, X., Zhang, S., Qiao, X., Cai, X., Xie, Q., 2010a. Aquatic photochemistry of fluoroquinolone antibiotics: kinetics, pathways, and multivariate effects of main water constituents. *Environ. Sci. Technol.* 44, 2400–2405.
- Ge, L., Chen, J., Zhang, S., Cai, X., Wang, Z., Wang, C., 2010b. Photodegradation of fluoroquinolone antibiotic gatifloxacin in aqueous solutions. *Chin. Sci. Bull.* 55, 1495–1500.
- Ge, L., Zhang, P., Halsall, C., Li, Y., Chen, C.E., Li, J., Sun, H., Yao, Z., 2019. The importance of reactive oxygen species on the aqueous phototransformation of sulfonamide antibiotics: kinetics, pathways, and comparisons with direct photolysis. *Water Res.* 149, 243–250.
- Gleckman, R., Alvarez, S., Jouber, D.W., 1979. Drug therapy reviews: Nitrofurantoin. *Am. J. Health Syst. Pharm.* 36, 342–351.
- Granucci, G., Persico, M., 2007. Critical appraisal of the fewest switches algorithm for surface hopping. *J. Chem. Phys.* 126, 134114.
- Guay, D.R., 2001. An update on the role of nitrofurans in the management of urinary tract infections. *Drugs* 61, 353–364.
- Gupta, K., Hooton, T.M., Roberts, P.L., Stamm, W.E., 2007. Short-course nitrofurantoin for the treatment of acute uncomplicated cystitis in women. *Arch. Intern. Med.* 167, 2207–2212.
- Härdle, W.K.S., Léopold, 2015. Applied Multivariate Statistical Analysis. Springer, Berlin Heidelberg.
- Hartigan, J.A., Wong, M.A., 1979. Algorithm as 136: a K-means clustering algorithm. *J. Appl. Stat.* 28, 100–108.
- Homem, V., Santos, L., 2011. Degradation and removal methods of antibiotics from aqueous matrices—a review. *J. Environ. Manag.* 92, 2304–2347.
- Hong, Y., Li, C., Zhang, G., Meng, Y., Yin, B., Zhao, Y., Shi, W., 2016. Efficient and stable Nb 2 O 5 modified g-C 3 N 4 photocatalyst for removal of antibiotic pollutant. *Chem. Eng. J.* 299, 74–84.
- Hoseini, M., Safari, G.H., Kamani, H., Jaafari, J., Ghanbarain, M., Mahvi, A.H., 2014. Sonocatalytic degradation of tetracycline antibiotic in aqueous solution by sonocatalysis. *Toxicol. Environ. Chem.* 95, 1680–1689.
- Hu, D., Liu, Y.F., Sobolewski, A.L., Lan, Z., 2017. Nonadiabatic dynamics simulation of keto isocytosine: a comparison of dynamical performance of different electronic-structure methods. *Phys. Chem. Chem. Phys.* 19, 19168–19177.
- Jain, A.K., 2010. Data clustering: 50 years beyond K-means. *Pattern Recogn. Lett.* 31, 651–666.
- Johnson, M.A., Martínez, T.J., 2012. Annual review of physical chemistry preface. *Annu. Rev. Phys. Chem.* 63, V–VI.
- Kasha, M., 1950. Characterization of electronic transitions in complex molecules. *Discuss. Faraday Soc.* 9, 14–19.
- Klán, P., Witz, J., 2009. Photochemistry of Organic Compounds: from Concepts to Practice. John Wiley & Sons.
- Kranz, J.J., Elstner, M., 2016. Simulation of singlet exciton diffusion in bulk organic materials. *J. Chem. Theor. Comput.* 12, 4209–4221.
- Lan, Z., Fabiano, E., Thiel, W., 2009. Photoinduced nonadiabatic dynamics of pyrimidine nucleobases: on-the-fly surface-hopping study with semiempirical methods. *J. Phys. Chem. B* 113, 3548–3555.
- Lastre-Acosta, A.M., Cristofoli, B.S., Parizi, M.P.S., do Nascimento, C.A.O., Teixeira, A.C.S.C., 2020. Photochemical persistence of sulfa drugs in aqueous medium: kinetic study and mathematical simulations. *Environ. Sci. Pollut. Res.* 1–9.
- Li, K., Zhang, P., Ge, L., Ren, H., Yu, C., Chen, X., Zhao, Y., 2014. Concentration-dependent photodegradation kinetics and hydroxyl-radical oxidation of phenicol antibiotics. *Chemosphere* 111, 278–282.
- Li, Y., Wei, X., Chen, J., Xie, H., Zhang, Y.N., 2015. Photodegradation mechanism of sulfonamides with excited triplet state dissolved organic matter: a case of sulfadiazine with 4-carboxybenzophenone as a proxy. *J. Hazard Mater.* 290, 9–15.
- Li, Y., Chen, J., Qiao, X., Zhang, H., Zhang, Y.N., Zhou, C., 2016a. Insights into photolytic mechanism of sulfapyridine induced by triplet-excited dissolved organic matter. *Chemosphere* 147, 305–310.
- Li, Y., Qiao, X., Zhang, Y.N., Zhou, C., Xie, H., Chen, J., 2016b. Effects of halide ions on photodegradation of sulfonamide antibiotics: formation of halogenated intermediates. *Water Res.* 102, 405–412.
- Li, X., Xie, Y., Hu, D., Lan, Z., 2017. Analysis of the geometrical evolution in on-the-fly surface-hopping nonadiabatic dynamics with machine learning dimensionality reduction approaches: classical multidimensional scaling and isometric feature mapping. *J. Chem. Theor. Comput.* 13, 4611–4623.
- Li, X., Hu, D., Xie, Y., Lan, Z., 2018. Analysis of trajectory similarity and configuration similarity in on-the-fly surface-hopping simulation on multi-channel nonadiabatic photoisomerization dynamics. *J. Chem. Phys.* 149, 244104.
- Liu, F., Ying, G.G., Tao, R., Zhao, J.L., Yang, J.F., Zhao, L.F., 2009. Effects of six selected antibiotics on plant growth and soil microbial and enzymatic activities. *Environ. Pollut.* 157, 1636–1642.
- Lorenzo, F., Navaratnam, S., Edge, R., Allen, N.S., 2008. Primary photophysical properties of moxifloxacin—a fluoroquinolone antibiotic. *Photochem. Photobiol.* 84, 1118–1125.
- Lorenzo, F., Navaratnam, S., Edge, R., Allen, N.S., 2009. Primary photoprocesses in a fluoroquinolone antibiotic sarafloxacin. *Photochem. Photobiol.* 85, 886–894.
- Mai, S., Marquetand, P., González, L., 2018. Nonadiabatic dynamics: the SHARC approach. *Wires. Comput. Mol. Sci.* 8, e1370.
- Parra, G.G., Ferreira, L.P., Codognato, D.C.K., Cavalheiro, C.C.S., Borissevitch, I., 2017. Characteristics of the excited states of Nitrofurantoin, an anti-inflammatory and photoactive nitrofuran derivative. *J. Lumin.* 185, 10–16.
- Persico, M., Granucci, G., 2018. Photochemistry: A Modern Theoretical Perspective. Springer.
- Richter, M., Marquetand, P., González-Vázquez, J., Sola, I., González, L., 2011. SHARC: ab initio molecular dynamics with surface hopping in the adiabatic representation including arbitrary couplings. *J. Chem. Theor. Comput.* 7, 1253–1258.
- Rohrdanz, M.A., Zheng, W., Clementi, C., 2013. Discovering mountain passes via torchlight: methods for the definition of reaction coordinates and pathways in complex macromolecular reactions. *Annu. Rev. Phys. Chem.* 64, 295–316.
- Roos, B.O., Lawley, K.P., 1987. The complete active space self-consistent field method and its applications in electronic structure calculations. *Adv. Chem. Phys.* 69, 399–445.
- Sarle, W.S., Kaufman, L., Rousseeuw, P.J., 1991. Finding groups in data: an introduction to cluster analysis. *J. Am. Stat. Assoc.* 86, 830–832.
- Singh, N., Gandhi, S., McArthur, E., Mois, L., Jain, A.K., Liu, A.R., Sood, M.M., Garg, A.X., 2015. Kidney function and the use of nitrofurantoin to treat urinary tract infections in older women. *Can. Med. Assoc. J.* 187, 648–656.
- Szabó-Bárdos, E., Cafuta, A., Hegedűs, P., Fónagy, O., Kiss, G., Babić, S., Škorić, I., Horváth, O., 2020. Photolytic and photocatalytic degradation of nitrofurantoin and its photohydrolytic products. *J. Photochem. Photobiol. A* 386, 112093.

- Tannor, D., 2007. Introduction to Quantum Mechanics: a Time-dependent Perspective. University Science Books.
- Tripathi, V., Tripathi, P., 2017. Antibiotic Resistance Genes: an Emerging Environmental Pollutant. Perspectives in Environmental Toxicology. Springer, Cham, pp. 183–201.
- Tully, J.C., 1990. Molecular-dynamics with electronic-transitions. *J. Chem. Phys.* 93, 1061–1071.
- Wayne, R.P., 2005. Environmental Photochemistry Part II. Springer, Berlin Heidelberg.
- Wei, X., Chen, J., Xie, Q., Zhang, S., Ge, L., Qiao, X., 2013. Distinct photolytic mechanisms and products for different dissociation species of ciprofloxacin. *Environ. Sci. Technol.* 47, 4284–4290.
- Werner, J.J., Arnold, W.A., McNeill, K., 2006. Water hardness as a photochemical parameter: tetracycline photolysis as a function of calcium concentration, magnesium concentration, and pH. *Environ. Sci. Technol.* 40, 7236–7241.
- Werner, J.J., Chintapalli, M., Lundeen, R.A., Wammer, K.H., Arnold, W.A., McNeill, K., 2007. Environmental photochemistry of tylosin: efficient, reversible photoisomerization to a less-active isomer, followed by photolysis. *J. Agric. Food Chem.* 55, 7062–7068.
- Werner, H.J., Knowles, P.J., Knizia, G., Manby, F.R., Schutz, M., 2012. Molpro: a general-purpose quantum chemistry program package. *Wires. Comput. Mol. Sci.* 2, 242–253.
- Werner, H.J., Knowles, P.J., Manby, F.R., Black, J.A., Doll, K., HeBelmann, A., Kats, D., Köhn, A., Korona, T., Kreplin, D.A., Ma, Q., Miller III, T.F., Mitrushchenkov, A., Peterson, K.A., Polyak, I., Rauhut, G., Sibaev, M., 2020. The Molpro quantum chemistry package. *J. Chem. Phys.* 152, 144107.
- Wigner, E., 1932. On the quantum correction for thermodynamic equilibrium. *Phys. Rev.* 40, 749–759.
- Wohlgemuth, M., Bonačić-Koutecký, V., Mitić, R., 2011. Time-dependent density functional theory excited state nonadiabatic dynamics combined with quantum mechanical/molecular mechanical approach: photodynamics of indole in water. *J. Chem. Phys.* 135, 054105.
- Xu, J., Hao, Z., Guo, C., Zhang, Y., He, Y., Meng, W., 2014. Photodegradation of sulfapyridine under simulated sunlight irradiation: kinetics, mechanism and toxicity evolvement. *Chemosphere* 99, 186–191.
- Xu, C., Gu, F.L., Zhu, C., 2018. Ultrafast intersystem crossing for nitrophenols: ab initio nonadiabatic molecular dynamics simulation. *Phys. Chem. Chem. Phys.* 20, 5606–5616.